Hindawi
Journal of Nanomaterials
Volume 2020, Article ID 1523164, 14 pages
https://doi.org/10.1155/2020/1523164

Research Article

Synthesis of C-N-S-Tridoped TiO_2 from Vietnam Ilmenite Ore and Its Visible Light-Driven-Photocatalytic Activity for Tetracyline Degradation

Nguyen Thi Lan,[1] Vo Hoang Anh,[1] Hoang Duc An,[1] Nguyen Phi Hung,[1] Dao Ngoc Nhiem,[2] Bui Van Thang,[3] Pham Khac Lieu,[4] and Dinh Quang Khieu[5]

[1]*Qui Nhon University, 550000, Vietnam*
[2]*Institute of Materials Science, VAST, 10000, Vietnam*
[3]*Dong Thap University, 81000, Vietnam*
[4]*Hue University, 49000, Vietnam*
[5]*University of Sciences, Hue University, 49000, Vietnam*

Correspondence should be addressed to Nguyen Phi Hung; nguyenphihung@qnu.edu.vn
and Dinh Quang Khieu; dqkhieu@hueuni.edu.vn

Received 3 January 2020; Revised 18 February 2020; Accepted 24 February 2020; Published 16 March 2020

Guest Editor: Yong Hu

In this study, C-N-S-tridoped TiO_2 composite was fabricated from TiO_2 prepared from ilmenite ore and thiourea by means of hydrothermal method. The obtained material was characterized by X-ray diffraction, Raman scattering spectroscopy, UV-Vis diffuse reflectance spectroscopy, nitrogen adsorption-desorption isotherms, scanning electron microscopy (SEM), transmission electron microscopy (TEM), and X-ray photoelectron spectroscopy (XPS). It was found that C-N-S-tridoped TiO_2 material has a large specific surface area, showing good photocatalytic activity on the degradation of antibiotic tetracycline in visible light region. The study on the mechanism of tetracycline photodegradation using the liquid chromatography with mass spectrometry was performed. It was found that tetracycline has been degraded over C-N-S-tridoped TiO_2 catalyst into many different intermediates which can eventually be converted into CO_2 and H_2O. The kinetics of photocatalytic decomposition of tetracycline were investigated. In addition, the obtained material could catalyze well the degradation of other antibiotics (ciprofloxacin and chloramphenicol) and dyes (rhodamine-B, methylene blue, and organe red). The catalyst was stable after five recycles with slight loss of catalytic activity, which indicates great potential for practical application of C-N-S-tridoped TiO_2 catalyst in treatment of wastewater containing tetracycline in particular or antibiotics in general.

1. Introduction

Tetracycline (denoted as TC) is one of the widely used antibiotics in veterinary medicine and aquaculture [1]. Due to poor absorption, most of them are not metabolized and excreted in the faces and urine as the original compounds. Tetracycline is usually detected at a concentration of 0.07-1.34 μg/L in surface water samples. The most dangerous effect of antibiotics in the environment is to create favorable conditions for the development of resistant strains of bacteria and cause the current phenomenon of antibiotic resistance [2]. Therefore, the elimination of tetracycline should be of considerable concern. Most of the amount of tetracycline detected in surface water, drinking water, and mud is due to the ineffective elimination of traditional and biological methods [1, 3]. In order to reduce the amount of tetracycline released into the environment, new treatment methods need to be developed. Advanced oxidation processes (AOPs) such as photochemical processes [1, 3], ozonation [4], ultrasonic waves [5], and Fenton processes [6] are considered as effective technologies to decompose antibiotic pollutants in aqueous solution. Among the AOPs, photocatalytic process based on titanium dioxide is one of the most promising technologies. TiO_2, with the preeminent properties, such as high

photocatalytic activity and super wetting, is very durable and nontoxic and has high reserves; it has been studied and applied widely [7]. However, with a band gap of about 3.2-3.5 eV, TiO_2 material can only give a catalytic effect in the ultraviolet (UV) light region. The portion of UV radiation in the solar spectrum to the earth's surface is only about 5%, so the use of this source of radiation for TiO_2 photocatalytic treatment is limited. In order to expand the use of solar radiation energy in the visible light area into the photocatalytic reaction, it is necessary to reduce the band gap energy of TiO_2 or shift the light absorption of TiO_2 from the UV to the visible region. Many studies have suggested that TiO_2 doped with nonmetal elements such as C, F, N, and S can extend the absorption spectrum to the visible light region [8–11].

Recently, the simultaneous doping of two or three nonmetals as a promising strategy to increase the photocatalytic activity of TiO_2 in the visible region exhibits higher photocatalytic activity than that of TiO_2 doping an element [12]. Zhou and Yu [13] reported that TiO_2 crystals simultaneously modified C, N, and S by solid phase reaction exhibited high photocatalytic activity for formaldehyde decomposition in visible light region. Ao et al. [14] prepared the C-N-S-tridoped TiO_2 through sol-gel method combined with surfactant cetyltrimethylammonium bromide (CTAB) as a soft template. Photocatalytic activity is assessed by the decomposition of Reactive Dyes Brilliant Red X-3B in aqueous solution. Wang et al. [15] prepared C-N-S-doped TiO_2 nanocrystals by hydrothermal method in the presence of TiO_2 and L-cysteine biological molecule. L-cysteine not only provided a source of carbon, sulfur, and nitrogen, but also controlled the final product of crystalline and morphological phases. The high activity of this catalyst in visible region is due to the synergic effect of the large surface area, the red shift at the absorption edge, the strong absorption in the visible light zone, and the phase structure mixture of the material.

In the present study, TiO_2 was prepared from ilmenite ore by using sulfuric acid method, then doping of C, N, and S elements into TiO_2 was performed through the hydrothermal process of TiO_2 and thiourea. Photocatalytic decomposition reaction in the visible region of tetracycline on C-N-S-tridoped TiO_2 composite was investigated.

2. Experimental

2.1. Materials and Synthesis. Ilmenite ore was provided kindly by the Binh Dinh company (Vietnam). The chemical composition analyzed by Atomic Absorption Spectroscopy (AAS) was listed in Table 1.

Sulfuric acid (H_2SO_4, 98%), thiourea (CH_4N_2S, 99%), methylene blue ($C_{16}H_{18}N_3SCl$, 99%), and organe red ($C_{16}H_{11}N_2NaO_4S$, 99%) were purchased from the Factory Co., Ltd. (China); rhodamine-B ($C_{28}H_{31}ClN_2O_3$, Merck, 99%), tetracycline hydrochloride ($C_{22}H_{24}O_8N_2{\cdot}HCl$, 96.09%), ciprofloxacin hydrochloride ($C_{17}H_{18}FN_3O_3{\cdot}HCl$ 94.73%), and chloramphenicol ($C_{11}H_{12}Cl_2N_2O_5$, 99.62%) were obtained from the Drug Testing Institute in Ho Chi Minh city (Vietnam).

Table 1: The chemical composition of ilmenite.

Composition	TiO_2	FeO	Fe_2O_3	SiO_2	Other impurities
Wt%	49.54	32.69	11.21	0.21	6.35

2.1.1. Synthesis of $TiOSO_4$ Material from Ilmenite Ore. Add 137.88 mL sulfuric acid solution (90%) to a 500 mL heat-resistant flask containing 50 grams of ilmenite ore. The mixture was heated for 1 hour with stirring at 200-210°C on a sand bath and then add 380 mL of 0.005 M H_2SO_4 under magnetic stirring for 3 hours at 70°C. Let the mixture settle for about 8 hours and remove the solid phase. Add 7.6 grams of iron billet to the obtained liquid for reducing Fe^{3+} to Fe^{2+} [16, 17]. This solution was concentrated until scum formation. Then cool the solution at a temperature of about -2°C to -5°C for 8 hours. The precipitate was separated, and $TiOSO_4$ solution was obtained.

2.1.2. Synthesis of C-N-S-Tridoped TiO_2 Materials. Take 2.27 grams of $TiOSO_4$ and a defined amount of thiourea (with molar ratio of thiourea: $TiO_2 = 2 : 1$) into a teflon flask, then dissolve with distilled water. Put the teflon bottle in the autoclave at 180°C for 12 hours. After the hydrothermal process, the autoclave was naturally cooled to room temperature. Filter the white precipitate and wash several times with distilled water until the filtrate has a constant pH. The product is dried and calcined at 400-700°C for 1 hour to obtain the C-N-S-tridoped TiO_2 (denoted as TH-TiO_2-a (a = 400, 500, 600, and 700°C). TiO_2 samples were also prepared as the abovementioned procedure but without adding thiourea.

2.2. Catalytic Activity. The catalytic activity of TiO_2 or TH-TiO_2 was estimated through the decomposition of tetracycline (30 mg/L) and the catalytic mass (0.6 g/L). The mixture was stirred in the dark for 30 minutes to reach the absorption/desorption equilibrium, then illuminated with a 60 W filament lamp (filter cutoff $\lambda < 420$ nm). The remaining tetracycline concentration was determined by HPLC-UV method on Thermo Scientific series 3300 HPLC (Thermo Scientific Technologies, CA, USA) ($\lambda_{max} = 355$ nm).

2.3. Methods of Analysis. The X-ray diffraction (XRD) was conducted in D8-Advance 5005 with Cu Kα $\lambda = 0.154$ nm. The element composition and oxidation state on the catalyst surface in the sample were determined by X-ray electron spectroscopy (XPS) (ESCALAB 250-Thermo VG, UK). The morphology and the element composition were measured by using scanning electron microscope (SEM) with energy dispersive X-ray spectroscopy (EDX) (Nova Nano SEM 450) and transmission electron microscopy (TEM) (JEOL JEM 1010). The photoluminescence (PL) was measured using a Hitachi F-7000 spectrophotometer over wavelength range of 375–600 nm with a 150 W xenon lamp. Raman spectrum and UV-Vis-DR were conducted by using T64000 Raman with 633 nm and GBC Instrument-2885, respectively. Textural properties of material samples were characterized by nitrogen adsorption/desorption isotherms method using Micromeritics ASAP 2000. The intermediates that appear

during tetracycline decomposition are determined by LC/MSD-Trap-SL method in combination with ESI method ionized mass spectrometry on Agilent. The mineralization of tetracycline in the photocatalytic degradation was monitored with TOC analyzer (Jena multi N/C 2100, Germany).

3. Results and Discussion

3.1. Characterization of Materials. The physical chemistry characterizations of TH-TiO_2 materials calcined at different temperature are presented in Figure S1–4 and Table S1. The primary experiments show that the TH-TiO_2 calcined at 500°C provided the highest photocatalytic activity (Figure S5). Therefore, the only discussion of TH-TiO_2 calcined at 500°C was focused in this text. The obtained materials were studied by XRD measurements (Figure 1). The diffractions of TiO_2 and TH-TiO_2 are observed at the same Bragg-angle and indexed as (101), (004), (200), (105), (211), (204), (116), (220), and (215) of the anatase phase [12, 18], indicating that the titanium oxide in anatase form is the main phase in the obtained samples. However, TH-TiO_2 prepared from hydrothermal process of TiO (SO_4) and thiourea possesses the lower intensities of anatase peaks compared to TiO_2 from hydrothermal process of only TiO (SO_4). The crystallite sizes of the samples could be estimated from the broadening of the X-ray diffraction peak according to Scherrer formula [19]. It was calculated that TiO_2 has an average crystallite size of 14.39 nm, and it decreases to 9.54 nm for TH-TiO_2 indicated that the tridoping of C, N, and S suppressed grain growth.

Raman spectrum (Figure 2) shows only the existence of 4 spectral bands at 144 cm^{-1}, 399 cm^{-1}, 399 cm^{-1}, 519 cm^{-1}, and 639 cm^{-1}, indicating that both TH-TiO_2 and TiO_2 have only anatase phase [20]. The peaks at 144 cm^{-1} (E_g) and 639 cm^{-1} (E_g) are related to the symmetrical stretching of the O-Ti-O bond in TiO_2 while the peak of 399 cm^{-1} (B1g) corresponds to the bending oscillation of the O-Ti-O bond, and 513 cm^{-1} (A1g) could be attributed to the asymmetric bending vibration of the O-Ti-O bond [21]. This result is consistent with XRD analysis.

The products prepared from ilmenite ore are expected to contain a certain amount of iron element. The element composition was investigated by EDX spectrum (Figure S6 and 7). It was found that the main elements in TiO_2 were Ti and O, and TH-TiO_2 were Ti, C, O, N, and S. It was notable that iron element was not detected in TiO_2 or TH-TiO_2 by XPS or EDX, this refuses the effect of iron oxide residue on catalytic activity of TiO_2 and TH-TiO_2.

The oxidation states of C, N, and S in TH-TiO_2 were studied by XPS spectra (Figure 3). The survey XPS spectrum (Figure 3(a)) presents Ti2p peaked at 459.36 eV, C1s at 284.70 eV, O1s at 531.00 eV, N1s at 400.30 eV, and S2p at 168.01 eV. The XPS level core spectrum of C1s (Figure 3(b)) shows a strong peak at 284.70 eV corresponding to the elemental carbon (graphite) that is formed by incomplete combustion of organic compounds under hydrothermal conditions. The spectral shoulders at 289.00 eV are associated with the presence of C=O bond of carbonate radicals on the catalytic surface [20]. Accord-

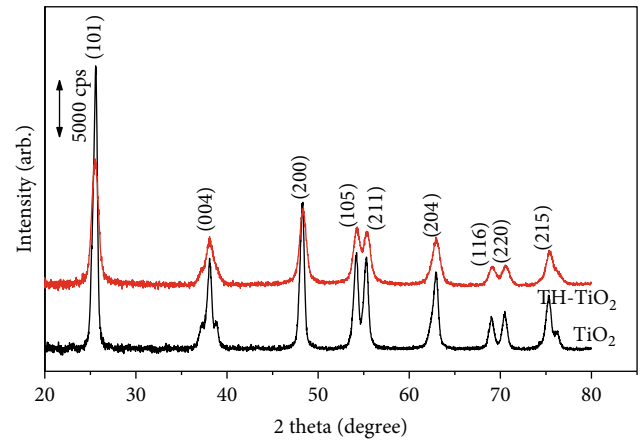

Figure 1: XRD patterns of TiO_2 and TH-TiO_2 samples.

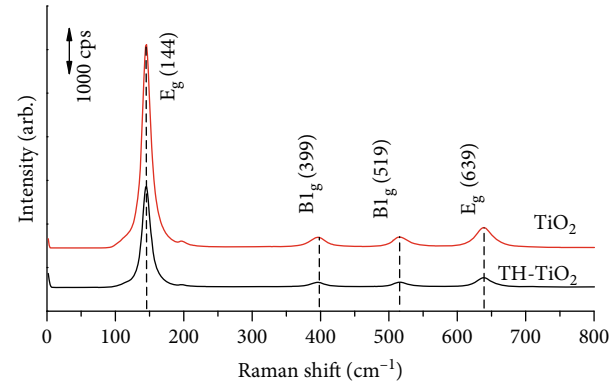

Figure 2: Raman spectra of TiO_2 and TH-TiO_2.

ing to the XPS spectrum at 286.2 eV, there was a replacement of some Ti atoms by C in lattice and forming Ti-O-C structure [18, 22]. The peak at 281 eV of the Ti-C bond was not found, indicating that C atom does not replace oxygen atoms in the TiO_2 lattice [23].

XPS core level spectrum of S2p (Figure 3(c)) with peaks at 168.7 and 169.50 eV corresponding to S^{6+} is replaced by Ti^{4+} [24–26]. No peak presenting for Ti-S links was found around 160-163 eV. This result is consistent with some previous studies which suggested that S^{+6} replacing Ti^{4+} in lattice is easier than replacing O^{2-} with S^{2-}[24, 27, 28]. This substitution also contributes to reducing the band gap energy of TiO_2 by introducing the interband gaps and lowering conduction band. The XPS core level spectrum of N1s (Figure 3(d)) shows that a wide maximum range of 399-401 eV corresponding to the replacement of N into oxygen position in TiO_2 network [29, 30] has contributed to increasing the valence band. Therefore, the band gap energy of TiO_2 decreases with nitrogen doping. The results of XPS analysis showed that carbon, nitrogen, and sulfur were added to the TiO_2 catalyst and their electronic structures change.

The UV-Vis diffuse reflectance spectroscopy (UV-Vis-DRS) is a useful technique to characterize the band gap energy of photocatalytic materials. In the present study, TC

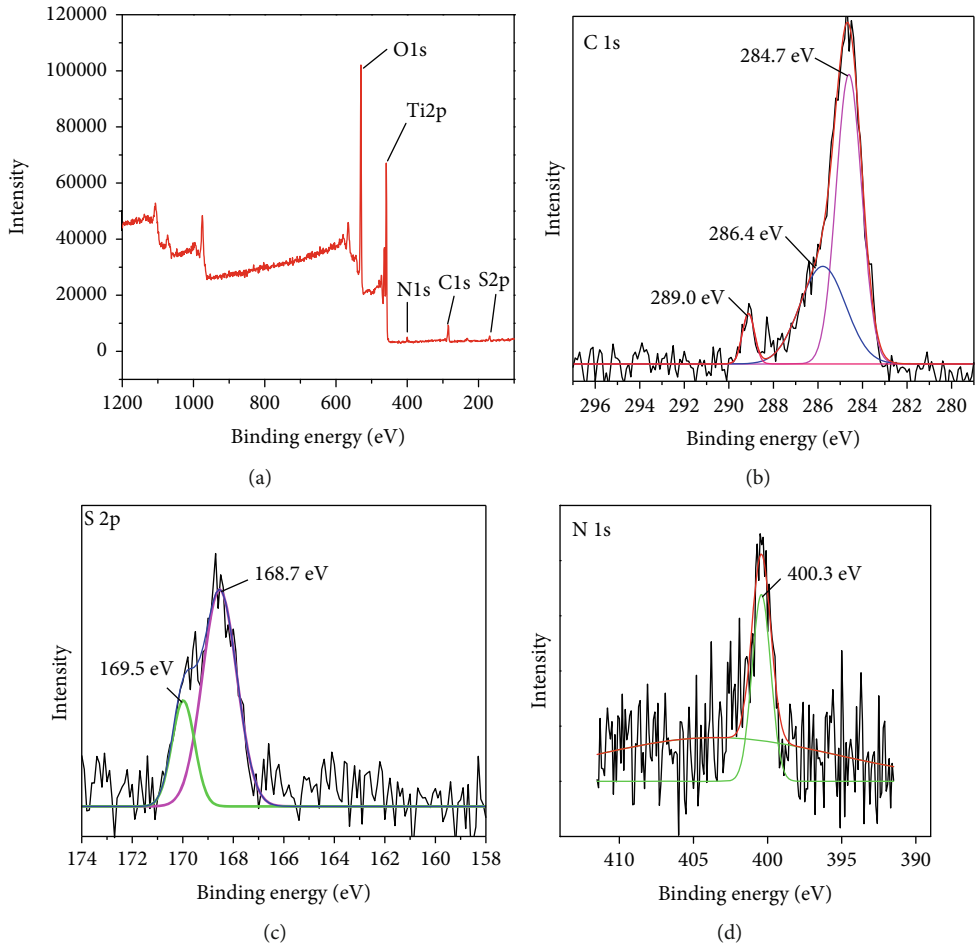

Figure 3: XPS spectrum of survey (a), C1p (b), S2p (c), and N1s (d) in sample TH-TiO_2.

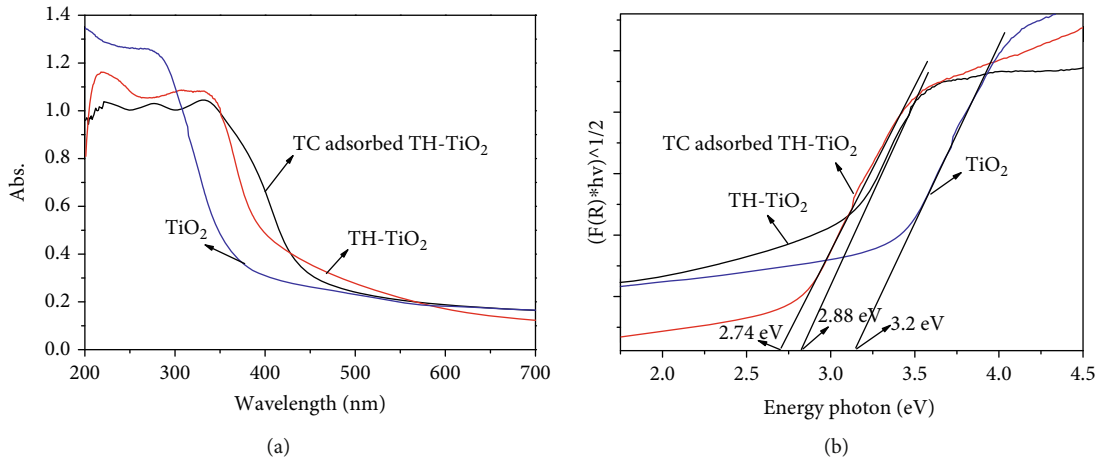

Figure 4: UV-Vis-DRS spectra (a) and the plot of Kubelka-Munk function for TiO_2, TC-adsorbed TH-TiO_2, and TH-TiO_2 (b).

adsorption of TH-TiO_2 in the dark was conducted; therefore, TH-TiO_2 adsorbing tetracycline at equilibrium (TC adsorbed TH-TiO_2), along with TiO_2 and TH-TiO_2, was characterized by means of UV-Vis-DRS. As can be seen from the figure, TH-TiO_2 sample had an absorption band shifting to higher wavelength compared with TiO_2. The band gap energy of TiO_2, TH-TiO_2, and TC-adsorbed TH-TiO_2 samples calculated by Kubelka-Munk function is 3.20, 2.88, and 2.74 eV, respectively (Figure 4(b)).

The red shift is thought to be C, N, and S doping to TiO_2 matrix, narrowing the band gap energy of the TiO_2 due to the occurrence of the hybridized states located in the band gap [31] or tetracyine as photosensitizer. The photoluminescence (PL) is widely used to study the recombination of photo-

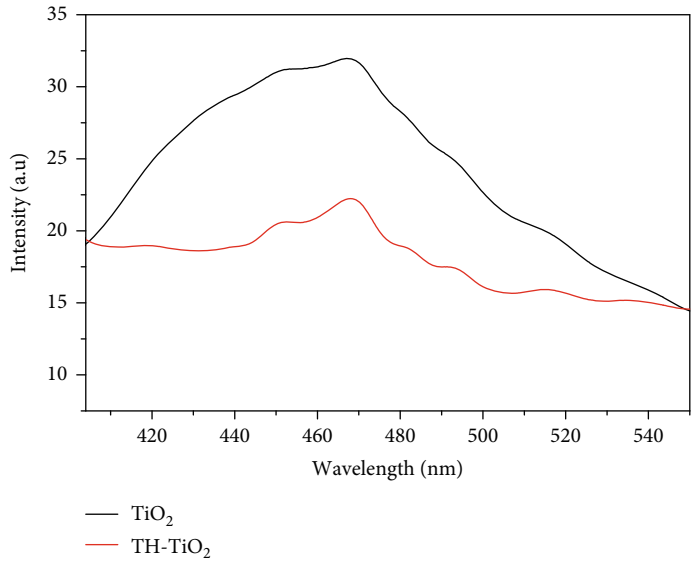

Figure 5: PL spectra of TiO_2 and TH-TiO_2.

induced electron/hole pairs. The PL spectra of TiO_2 and TH-TiO_2 materials are shown in Figure 5. The materials were excited at 404 nm with a strong emission peak at about 468 nm. It was found that there is a significant decrease in luminescence intensity of TH-TiO_2 compared to TiO_2. This demonstrates that the doping of C, N, and S into TiO_2 significantly improved the separation of photo-induced electrons, creating favorable conditions for reacting photo-generated holes and electrons with H_2O or oxygen to active radicals [23, 32].

From SEM images shown in Figures 6(a) and 6(b), it is observable that both of the pure and doped TiO_2 samples perform similar morphology which includes secondary particles with size varying from 500 to 600 nm constructed from primary subparticles. The only difference, however, could be observed is that, compared to pure sample, TH-TiO_2 exhibits significantly rougher surface with higher porosity (as clearly seen in the consistent insets) which could be related to the gas formation due to decomposition of thiourea during synthesis condition. The construction of secondary particles from subone could be clarified in HR-TEM images (as shown in Figure 6(c)) which indicates that the size range of the primary particles is around 12 to 18 nm. The high magnification TEM image in Figure 6(d) displays the observable lattice fringe corresponding to (101) plane with distance of 0.352 nm which is confirmed by Fast Fourier Transforms (FFT) (insets). The acceptable crystallinity of obtained sample was further proved via Selected Area Electron Diffraction (SAED) (Figure 6(e)) which includes separated rings formed form clear spot. The corresponding lattice planes were also indexed in SAED pattern.

The textural properties of the obtained materials were investigated by means of nitrogen adsorption/desorption isotherms (Figure 7). The curves of both materials belong to type V with type H1 loops according to the IUPAC classification which are all characterized for the mesoporous structure formed by intersecting particles [33, 34]. The pore size curves exhibit the normal distribution with average sizes of 36.7 nm for TiO_2 and 13.8 nm for TH-TiO_2 (the inset of Figure 7). The doping of C, N, and S elements into TiO_2 matrix enhanced the specific surface area (the values of 36 $m^2 \cdot g^{-1}$ for TiO_2 and 74 $m^2.g^{-1}$ for TH-TiO_2 as calculated by BET model) and reduced also the pore size of TH-TiO_2.

3.2. Catalytic Activity. Some reports present that some natural minerals containing TiO shows photocatalytic activity in advanced oxidation process [35, 36]; therefore, the present raw ilmenite was conducted to test photocatalytic activity as a reference. Figure 8(a) presents the kinetics of TC degradation over TiO_2, raw ilmenite, and TH-TiO_2. As can be seen in the figure, ilmenite does not exhibit any photocatalytic activity toward to oxidize TC due to the chemical inert property of ilmenite mineral. For TH-TiO_2, the dark adsorption/desorption equilibrium is reached after 30 min, and it displays higher adsorption capacity than TiO_2 around 10% ($F = 14.69\%$ for TiO_2 and 24.63% for TH-TiO_2 in which $F = 100 \times C_t/C_0$, where C_0 and C_t are the initial concentration and at time t). It is worth noting that TH-TiO_2 yields a degradation efficiency of nearly 100% while TiO_2 yields only 50% after 120 min of visible light illumination. This may be due to larger surface area of TH-TiO_2 which increases the number of active sites for TC to adsorb and decompose. In the leaching experiment, the catalyst was filtered after 30 min, and the degradation of TC under illumination almost stops (Figure 8(a)). In addition, the degradation of TC without the catalyst is not observed after 120 min of illumination, revealing that TC is not photo-decomposed in the present condition. Therefore, it can be suggested that TH-TiO_2 acts as a heterogeneous catalyst in the TC photocatalytic degradation.

Figure 8(b) shows the UV-Vis spectra of TC solution during the photocatalytic degradation using visible light source. Two absorption bands peaked at 270 nm and 355 nm are observed. The former band is assigned to $\pi - \pi^*$

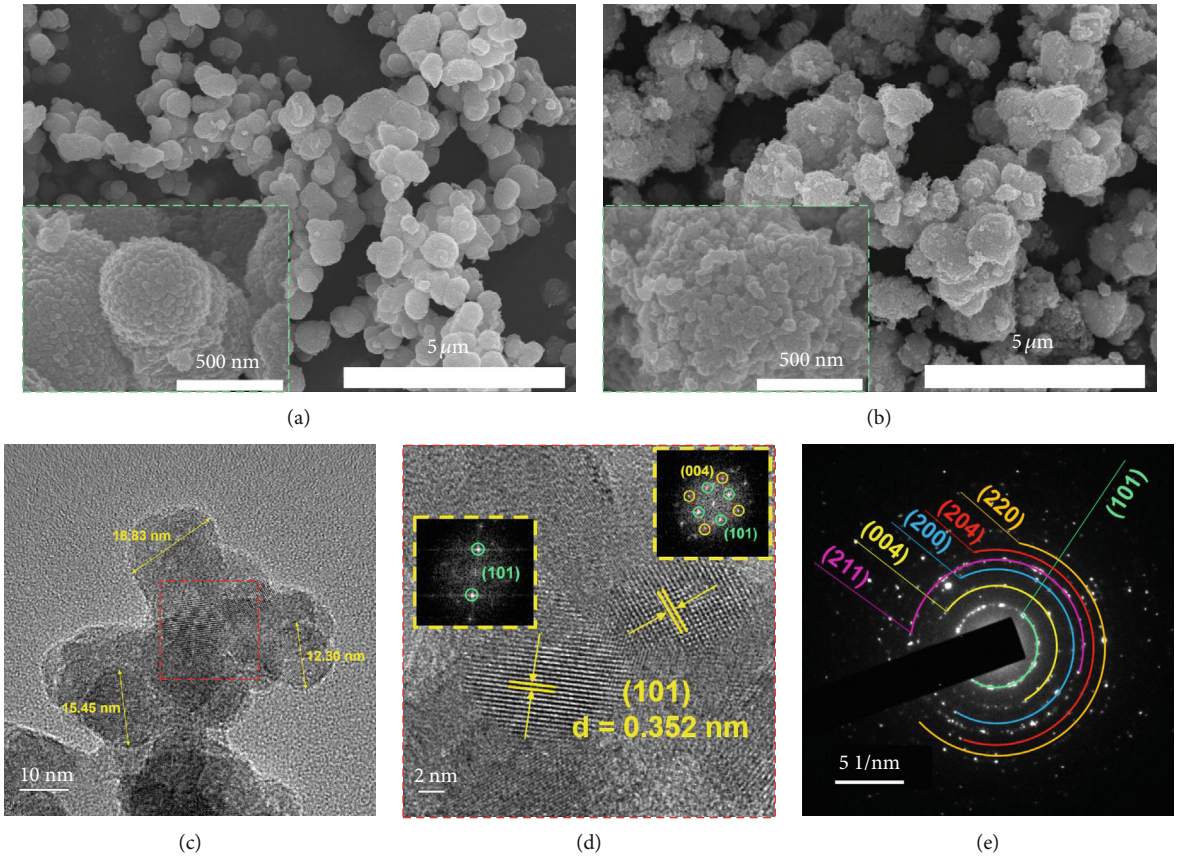

Figure 6: SEM images of (a) TiO_2, (b) TH-TiO_2 samples, (c, d) HR-TEM images with consistent Fast Fourier Transform (FFT) in insets, and (e) Selected Area Electron Diffraction (SAED) of TH-TiO_2.

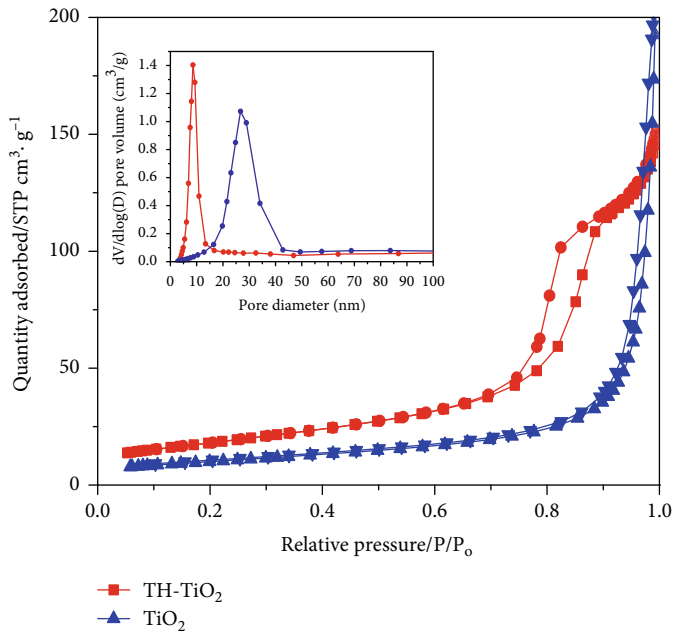

Figure 7: Nitrogen adsorption-desorption isotherms at 77 K; the inset presents pore size distribution of TiO_2 and TH-TiO_2.

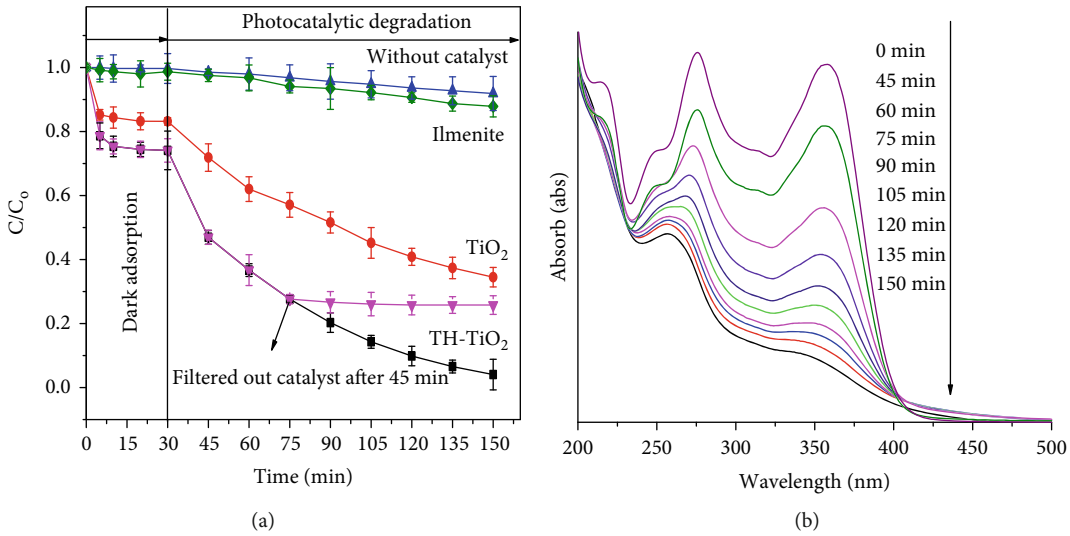

FIGURE 8: (a) Decolorization kinetics of TC over TiO_2 and TH-TiO_2 under visible light irradiation (conditions: $m_{catalyst} = 0.6\,g \cdot L^{-1}$; concentration of TC = 30 ppm; adsorption time = 30 min). (b) UV-Vis spectra of TC during irradiation time.

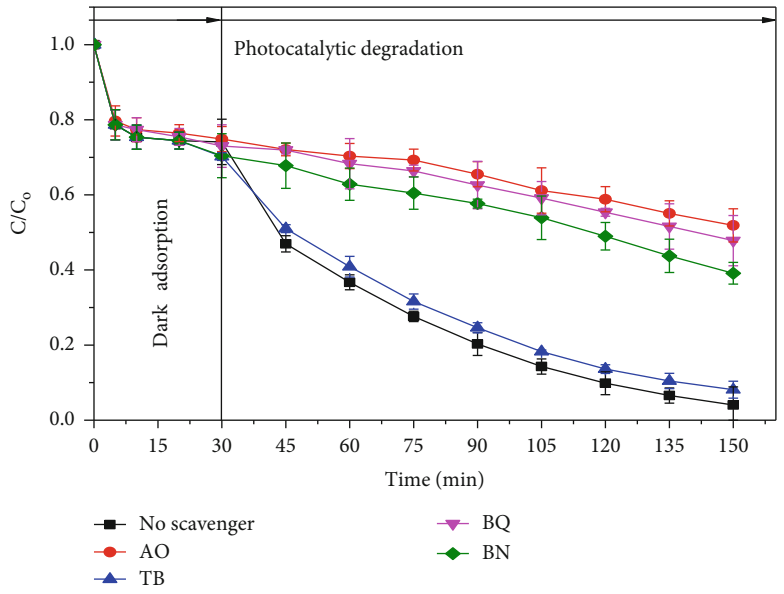

FIGURE 9: Kinetics of TC degradation on TH-TiO_2 in the presence of different scavengers.

transitions in benzene ring, and the latter is contributed to the conjugated double bonds. The decomposition of TC on TH-TiO_2 catalyst takes place quite quickly, after about 120 minutes of processing, the characteristic absorption peak of TC at 355 nm is almost disappeared. This result shows that TC decomposition has possible formed intermediates with smaller molecular masses.

It is well-known that free radicals such as photo-induced electrons and holes, $^{\bullet}OH$ and $O_2^{(\bullet-)}$, play a critical role in the degradation reactions of organic compounds. In particular, *tert*-butylic alcohol (TB) is used as a quencher for $^{\bullet}OH$ [37], 1,4-benzoquinon- (BQ-) quencher for $O_2^{(\bullet-)}$ [38, 39], ammonium oxalate- (AO-) quencher for H^+ [37, 39], and silver nitrate- (BN-) quencher for photosynthetic electrons e^- [40]. The 2 mL of 10 mM quenching solutions was added just after 30 min of dark adsorption. The effect of extinguishing agents on TC degradation performance is shown in Figure 9. In general, the presence of free radicals reduces the efficiency of TC degradation. AO (quenching h^+), BQ (quenching $O_2^{(\bullet-)}$), and BN (quenching e^-) reduce significantly the degradation rate of TC. However, TB seems not to affect TC degradation. This concludes that the free radicals (h^+; $O_2^{(\bullet\,-)}$; e^-) take mainly part in degradation reactions of TC while $^{\bullet}OH$ is negligible.

The tridoping of C, N, and S elements into TiO_2 lattice gives to rise new sublevels including S2p and C1s levels under Ti3d conduction band (CB); N2p level above the O2p valence band (VB) [41]. The sublevels of S2p and C1s served as trapping centers for photo-induced electrons that enhance the life times of the charge carriers due to the separation of

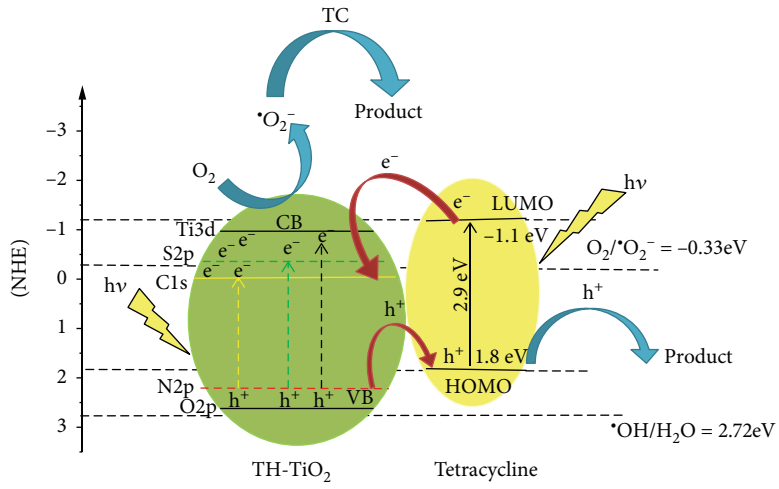

Scheme 1: The mechanisms of charge carrier migration and free radicals formation on TH-TiO_2 catalyst under visible light illumination.

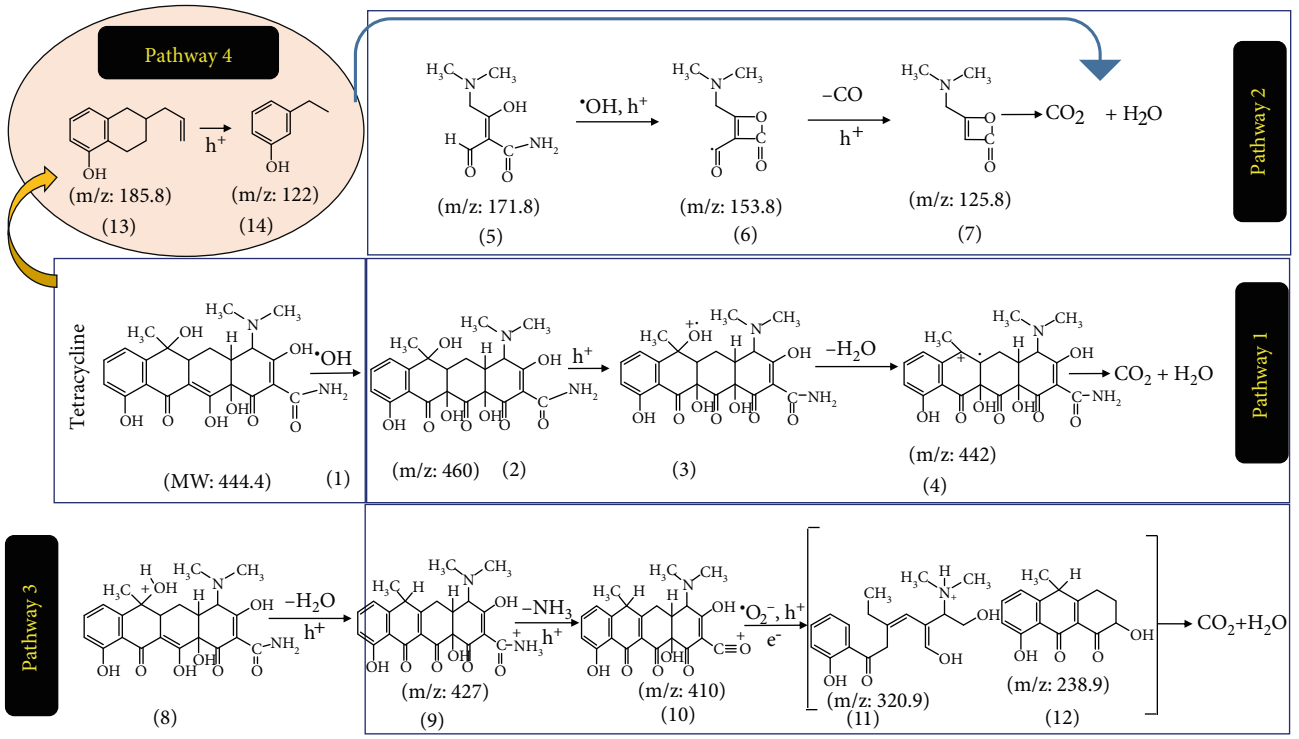

Scheme 2: The possible photocatalytic degradation pathways of TC on TH-TiO_2 catalyst.

hole-electron pairs (Scheme 1). Under visible illumination, TC acts as a photosensitser. TC molecule absorbs light and produces an electron (e^-) and hole (h^+) in LUMO and HOMO regions, respectively. The excited electrons in the LUMO migrated to the CB of the TH-TiO_2 because of the less positive potential of LUMO. E· ($O_2/O_2^{\bullet-}$, -0.033 eV), hence that photo-induced electrons could react with oxygen to provide $O_2^{\bullet-}$. Similarly, VB band of TH-TiO_2 (2.88 eV) was more positive than the potential of $^{\bullet}OH/OH^-$ (+2.27 eV), hence the photoinduced electrons are possible to oxidize H_2O to form $^{\bullet}OH$ radicals. These free radicals are strong oxidizing agent which could oxidize partially or complexly TC. The arguments are illustrated in Scheme 1 and in the following equations:

$$\begin{aligned}
\mathrm{TC} + h\nu &\longrightarrow \mathrm{TC}\left(e_{\mathrm{CB}}^- + h_{\mathrm{VB}}^+\right)\\
\text{Adsorbed TC}\left(e_{\mathrm{CB}}^- + h_{\mathrm{VB}}^+\right) + \mathrm{TH-TiO_2} &\longrightarrow \mathrm{TH-TiO_2}\left(e_{\mathrm{CB}}^-\right) + \mathrm{TC}\left(h_{\mathrm{VB}}^+\right)\\
\mathrm{TH-TiO_2}\left(e_{\mathrm{CB}}^-\right) + \text{adsorbed } O_2 &\longrightarrow {}^{\bullet}O_2^- \left(\text{or}\,{}^{\bullet}O^-\right) + \mathrm{TH-TiO_2}\\
H_2O &\longrightarrow H^+ + OH^-\\
H_2O + \mathrm{TH-TiO_2}\left(h_{\mathrm{VB}}^+\right) &\longrightarrow H^+ + {}^{\bullet}OH\\
{}^{\bullet}O_2^-, h^+ \text{ or } {}^{\bullet}OH + \text{adsorbed TC/TC}^* &\longrightarrow \text{degradation products}
\end{aligned} \quad (1)$$

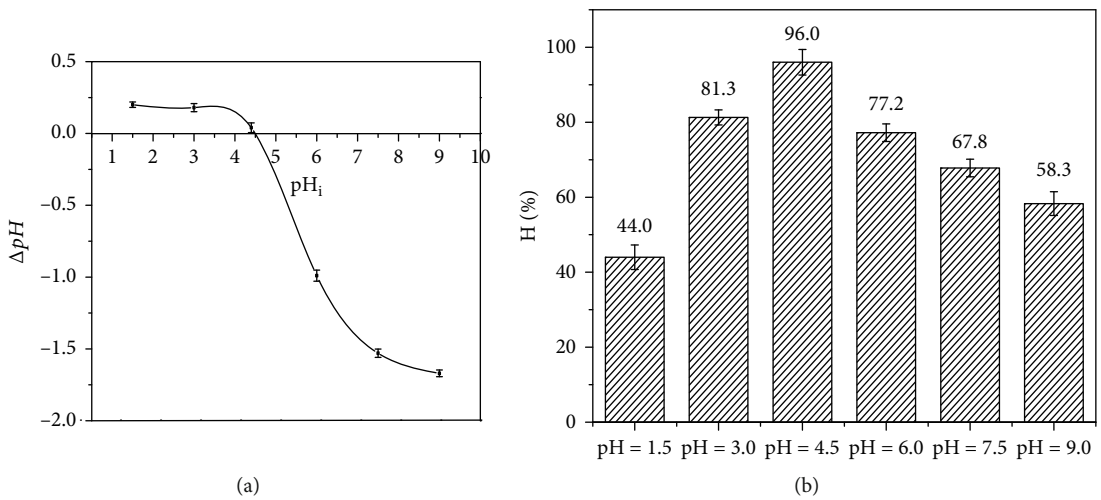

FIGURE 10: (a) Effect of pH on the TC degradation efficiency. (b) The pH_{PZC} determined by the pH drift method.

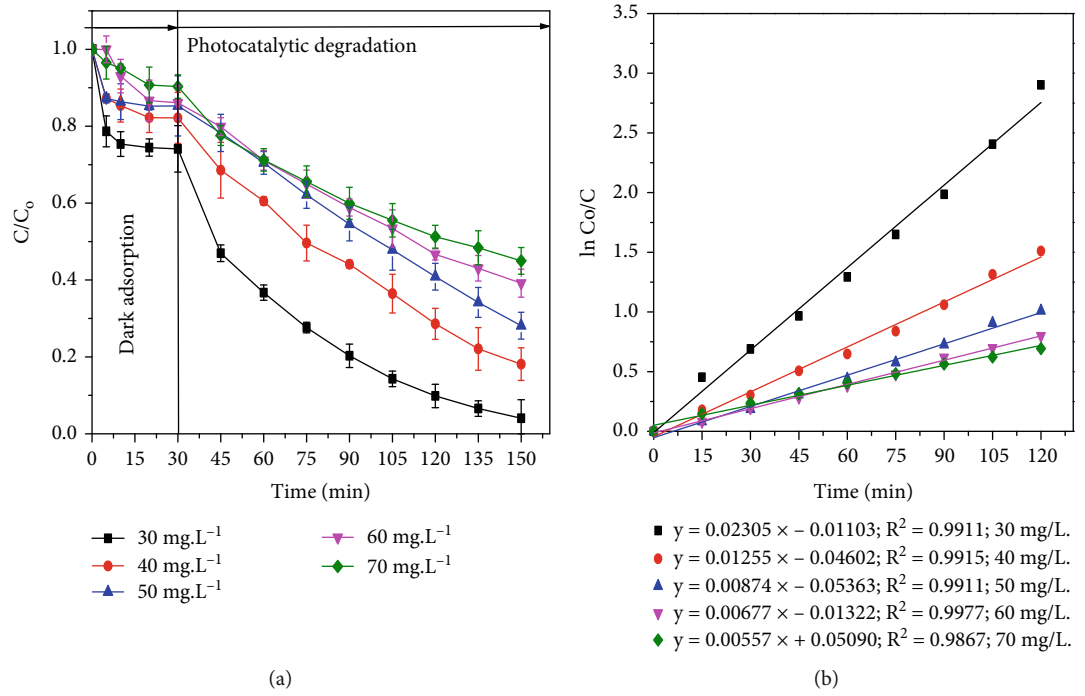

FIGURE 11: (a) Kinetics of TC decomposition reaction. (b) Plot of Langmuir-Hinshelwood model at different TC initial concentrations.

3.3. LC-MS Analysis. The mechanism of TC photodegradation on TH-TiO_2 catalyst was studied by using the liquid chromatography-mass spectrometry (LC-MS) (see Scheme 2 and Figure S8–10). The LC chromatography was conducted for the solution after reaction time of 30 min followed by mass spectrometry. The finding showed that the intermediates with retention times of 11.9, 16.4, and 30 have m/z values of 460, 427, 171.8, and 185.8, respectively, corresponding to molecular formulae of $C_{22}H_{24}O_9N_2$, $C_{22}H_{23}O_7N_2$, $C_7H_{12}O_3$, and $C_{13}H_{16}O$, respectively. Based on the previous works [42–44], the TC degradation is proposed as follows: initially TC (1) ($m/z = 444.4$) was added with the -OH group in the presence of free radicals $^{\bullet}OH$, and intermediate compound (2) ($m/z = 460$) was further dehydrated in the presence of h^+ to compound (4) ($m/z = 442$). These compounds break down the bonds to form (5), (13), and (14) by the presence of agents $^{\bullet}OH$ and H^+ [45] (Scheme S1).

For pathway 2 (Scheme S2), the ring opening products include compounds (5), (6), and (7), where (5) 4-dimethylamino-2-formyl-3-hydroxybut-2-enamide ($m/z = 171.8$) is formed as a result of direct oxidation from TC (1) or from (4). The presence of 4-((dimethylamino) methyl)-2H-oxet-2-one (7) ($m/z = 125.8$) is due to the internal molecular reaction chain of (5). The reaction mechanism can be described as follows: (step 1) OH (= C-OH) acts as a nucleophile agent, interacting with C = O in the amide function group according to SN2 (CO) mechanism. At the same time, the dehydro group and

Table 2: Comparison of rate constant of the present catalyst with published papers.

Catalyst	Conditions	F^* (%)	Rate constant k (min^{-1})	Ref.
N-TiO_2	(1) Light source: white led, 46 W·m^2 (2) C^o_{TC}: 5 mg·L^{-1} (3) $m_{catalyst}$: 0.3 g·L^{-1} (4) Time for dark adsorption: 45 min (5) Time for photocatalytic degradation: 200 min	74.0	0.012	[49]
N-TiO_2/rGO	(1) Light source: Xenon lamp, 300 W ($\lambda > 400$ nm) (2) C^o_{TC}: 10 mg·L^{-1} (3) $m_{catalyst}$: 1 g·L^{-1} (4) Time for dark adsorption: 30 min (5) Time for photocatalytic degradation: 60 min	98.0	0.057	[50]
Cu-TiO_2	(1) Light source: Xenon lamp, 1000 W ($\lambda > 420$ nm) (2) C^o_{TC}: 20 mg·L^{-1} (3) $m_{catalyst}$: 0.02 g·L^{-1} (4) Time for dark adsorption: 30 min (5) Time for photocatalytic degradation: 240 min	90.0	0.010	[51]
(Mo, C)-TiO_2/FTO	(1) Light source: Xenon lamp, 500 W ($\lambda > 400$ nm) (2) C^o_{TC}: 20 mg·L^{-1} (3) Time for dark adsorption: 60 min (4) Time for photocatalytic degradation: 100 min	89.5	0.022	[52]
$Ti_{0.9}Zr_{0.05}Sn_{0.05}$ O_2	(1) Light source: mercury low pressure lamp, 36 W (2) C^o_{TC}: 30 mg·L^{-1} (3) $m_{catalyst}$: 0.8 g·L^{-1} (4) Time for dark adsorption: 30 min (5) Time for photocatalytic degradation: 180 min	93.0	0.025	[53]
BiOCl/TiO_2/spinel	(1) Light source: Xenon lamp, ($\lambda > 400$ nm) (2) C^o_{TC}: 50 mg·L^{-1} (3) $m_{catalyst}$: 0.6 g·L^{-1} (4) Time for dark adsorption: 60 min (5) Time for photocatalytic degradation: 180 min	92.0	0.004	[54]
TH-TiO_2	(1) Light source: Xenon lamp, 45 W ($\lambda > 400$ nm) (2) C^o_{TC}: 30 mg·L^{-1} (3) $m_{catalyst}$: 0.6 g·L^{-1} (4) Time for dark adsorption: 30 min (5) Time for photocatalytic degradation: 150 min	100	0.023	The present work

$^*F = 100 \times (C_o - C_e)/C_o$ where C_o and C_e is the initial and final concentration.

aldehyde reaction also occurs under the action of $^{\bullet}$OH, H. (Step 2) compound (6) is formed unstably because containing single electrons tends to turn into (7) through decarbonylation process. In solution, the –OH (H_3C-C-OH) group of TC with high electron density will give way to H^+, then dehydration process with hydrogen displacement also happens to form a more stable structural compound (9) ($m/z = 427.0$) [46, 47] (Scheme S3). Compounds (11) ($m/z = 320.9$) and (12) ($m/z = 238.9$) are the result of NH_3 splitting and cutting off different bonds due to h^+ and e^-, $O^{2\bullet-}$. However, this process will not be clarified in this study because of the relatively complex mechanism and very short shelf life of intermediate compounds (pathway 3). Finally, compounds (13) and (14) are formed directly from TC or through intermediate compounds (4) (pathway 4). Besides, some compounds with small m/z (116.7, 91) were also found in the analysis process but were not identified because fragmentation data is relatively small. At the same time, the results of LC-ESI-MS analysis and the TOC measurement was subjected to reaction solution. Initial TOC was about 550 mg/L; however, it decreased 92% to 44 mg/L after 150 min treating, indicating the complete mineralization. It is concluded from LC-MS and TOC analysis that TC degradation over TH-TiO_2 catalyst proceeds via many different intermediates and they can eventually be converted into CO_2 and H_2O.

3.4. Kinetic Study. The pH of point of zero charge (pH_{PZC}) of TH-TiO_2 calculated by the pH drift method is 4.5

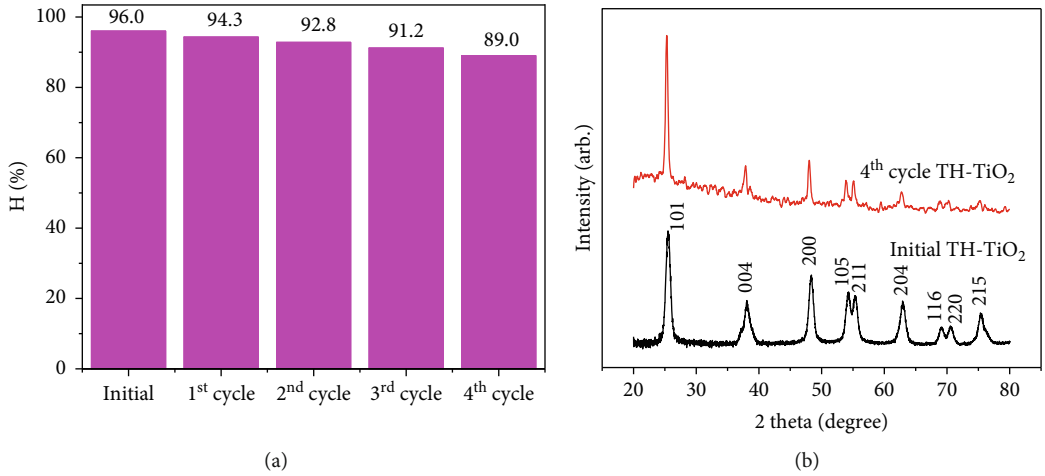

Figure 12: (a) TC degradation efficiency after four reuse cycles of TH-TiO_2. (b) XRD patterns of reused TH-TiO_2.

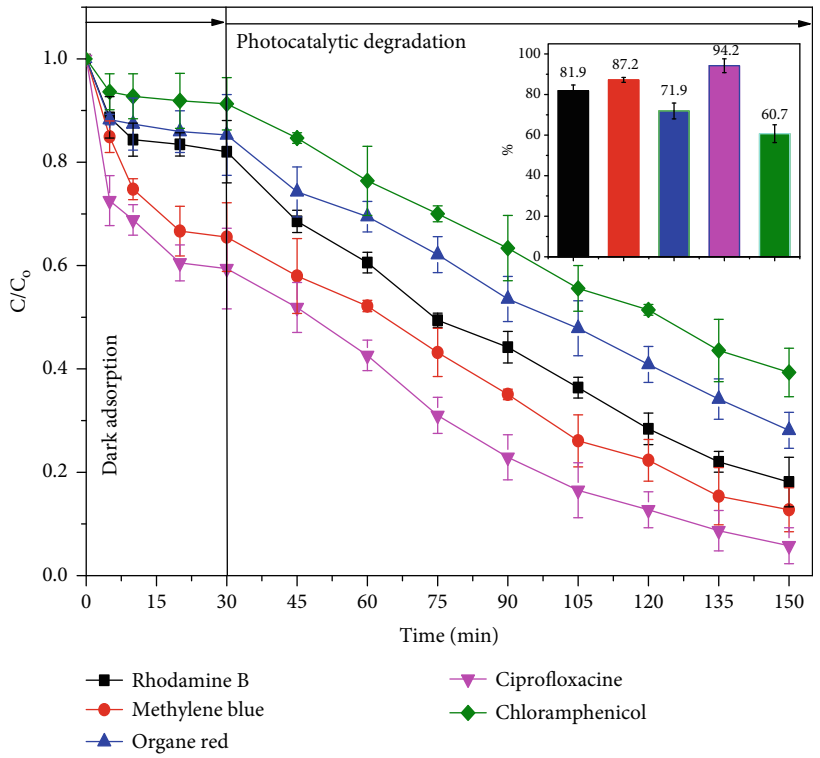

Figure 13: Kinetics of degradation reactions of some dyes and antibiotics over TH-TiO_2.

(Figure 10(a)). TC possesses three of pKa, i.e., pKa1 = 3.3, pKa2 = 7.68, and pKa3 = 9.7 [48].Then, TC is charged positively as pH is less than 3.3 and it is charged negatively as pH is more than 9.7. TC will be charged positively/negatively at pH within 3.3–7.68. The effect of pH on the TC degradation performance is illustrated in Figure 10(b). As can be seen from the figure, the TC degradation efficiency increases with an increase in pH and peaks around pH 4–6 and significantly decreases with further increase in pH. At pH is too low (<3.3) or too high (>7.68), the degradation efficiency was decreased because pulse interaction of the same charge carries. At a range of pH of 3-6, isoelectronic interaction is predominated compared with pulse one.

3.5. Effect of Initial TC Concentrations. In this experiment, the initial TC concentration varied from 30 to 70 mg·L^{-1}, the other experimental conditions remained the same. It was found that when increasing the initial TC concentration from 30 to 70 mg·L^{-1}, decomposition efficiency decreases significantly from 96% to 55% after 120 minutes of visible light illumination (Figure 11(a)). The catalytic reduction performance by TC concentrations can be explained by the fact that the higher initial TC concentration, the more TC molecules adsorbed on the surface of the TH-TiO_2. With a fixed amount of catalyst, excessive TC adsorption causing blockage of active sites on the substrate surface leads to negatively affecting photocatalytic activity. The Langmuir-Hinshelwood model

was employed to analyze the kinetics data in which the linear plot of $\ln(C_t/C_o)$ *vs.t* is constructed. Figure 11(b) presents the Langmuir-Hinshelwood plots at different concentrations. The high determination coefficients, R^2 (0.99–1) confirm that the kinetic degradation reaction of TC over TH-TiO_2 fixed well the Langmuir-Hinshelwood model.

Table 2 presents the rate constants of TC degradation reaction over different catalysts. Although the comparison is lame because the reaction conditions are not the same. However, from Table 1, it can be seen that the rate constant of TH-TiO_2 is relative high compared to previous studies.

3.6. Reusability. Reusability is one of the very important factors when deciding to choose a catalyst for economic and environmental purposes. The used TH-TiO_2 material was washed many times with distilled water and dried at 80°C for 12 hours for regeneration. The TC degradation efficiency over reused catalyst is presented in Figure 12(a). This result shows a slight reduction in TC decomposition efficiency, but after four reuse times, effective TC decomposition still reached over 89.0%. The XRD patterns of TH-TiO_2 (Figure 12(b)) seem slightly changeable indicating TH-TiO_2 possessed excellent structural stability after the regeneration process.

3.7. Catalytic Decomposition of Other Compounds. The photocatalytic activity of TH-TiO_2 was tested for some dyes and antibiotics (Figure 13). It was found that the present TH-TiO_2 could catalyze excellently for dyes (rhodamine-B, methylene blue, and organe red) or antibiotics (ciprofloxacin and chloramphenicol). This offers a potential application of TH-TiO_2 material in the removal of antibiotics in particular and organic pollutants in general from shrimp pond wastewater.

4. Conclusions

The tridoping of S, N, and C into TiO_2 extracted from ilmenite ore by hydrothermal process with thiourea was demonstrated. The S-N-C-tridoped TiO_2 exhibited an excellent catatalytic activity toward the complete minerazation of tetracyline. The possible pathways of tetracyline phototocatalytic degradation over obtained catalyst include hydroxylation, dealkylation, and dehydration via intermediates with smaller molecular mass to final products of CO_2 and water. In addition, the S-N-C-tridoped TiO_2 are potential for photocatalytic degradation of other antibiotics (ciprofloxacin and chloramphenicol) and some dyes (rhodamine-B, methylene blue, and organe red).

Data Availability

The data used to support the findings of this study are available from the corresponding author upon request.

Conflicts of Interest

The authors declare that they have no conflicts of interest.

Acknowledgments

The authors would sincerely like to thank the Team of VLIR-UOS (code ZEIN2016PR431) and the Vietnam Ministry of Education and Training (code B2019-DQN-13) for their financial support.

Supplementary Materials

Figure S1: XRD patterns of TH-TiO2-*a* (*a* = 400, 500, 600, and 700°C). Figure S2: nitrogen adsorption/desorption isotherms of TH-TiO2-*a* (*a* = 400, 500, 600, and 700°C). Figure S3: UV-Vis DRS spectra of TH-TiO2-*a* (*a* = 400, 500, 600, and 700°C) and TiO2. Figure S4: the Kubelka-Munk plots for TH- TH-TiO2-*a* (*a* = 400, 500, 600, and 700°C) and TiO2. Figure S5: the plot of C/C_o*vs.* time for adsorption and photocatalytic reaction or TiO2 và TH-TiO2-*a* (*a* = 400, 500, 600, and 700°C), (C_o = 30 mg/L and $m_{catalyst}$ = 0.6 gram·L-1); *V* = 100 mL) Figure S6: EDX spectrum and the elements content of TH-TiO2. Figure S7: EDX spectrum and the elements content of TiO2. Figure S8: LC diagram at the retention time of 11.9 min (upper) and its mass spectrum (lower). Figure S9: LC diagram at the retention time of 30 min (upper) and its mass spectrum (lower). Figure S10: LC diagram at the retention time of 16.4 min (upper) and its mass spectra (lower). Table S1: physical chemistry properties of TH-TiO2-*a*. Scheme S1: the proposed fragmentation mechanism of the compound at the retention time of 11.9 min. Scheme S2: the proposed fragmentation mechanism of the compound at the retention time of 30 min. Scheme S3: the proposed fragmentation mechanism of the compound at the retention time of 16.4 min. *(Supplementary Materials)*

References

[1] R. A. Palominos, M. A. Mondaca, A. Giraldo, G. Peñuela, M. Pérez-Moya, and H. D. Mansilla, "Photocatalytic oxidation of the antibiotic tetracycline on TiO_2 and ZnO suspensions," *Catalysis Today*, vol. 144, no. 1-2, pp. 100–105, 2009.

[2] M. Addamo, V. Augugliaro, A. D. Paola et al., "Removal of drugs in aqueous systems by photoassisted degradation," *Journal of Applied Electrochemistry*, vol. 35, no. 7-8, pp. 765–774, 2005.

[3] P. Wang, P. S. Yap, and T. T. Lim, "C-N-S tridoped TiO_2 for photocatalytic degradation of tetracycline under visible-light irradiation," *Applied Catalysis A: General*, vol. 399, no. 1-2, pp. 252–261, 2011.

[4] M. H. Khan, H. Bae, and J. Y. Jung, "Tetracycline degradation by ozonation in the aqueous phase: proposed degradation intermediates and pathway," *Journal of Hazardous Materials*, vol. 181, no. 1-3, pp. 659–665, 2010.

[5] S. Dobaradran, R. Nabizadeh, A. H. Mahvi et al., "Survey on degradation rates of trichloroethylene in aqueous solutions by ultrasound," *Iranian Journal of Environmental Health Science and Engineering*, vol. 7, no. 4, pp. 307–312, 2010.

[6] A. Ž. Gotvajn, M. Bistan, T. Tišler, A. J. Englande, and J. Zagorc-Končan, "The relevance of bisphenol A adsorption during Fenton's oxidation," *International Journal of*

Environmental Science and Technology, vol. 10, no. 6, pp. 1141–1148, 2013.

[7] A. Fujishima, K. Hashimoto, and T. Watanabe, "TiO_2 photocatalysis fundamentals and applications," in *A Revolution in Cleaning Technology*, pp. 14–21, 1999.

[8] P. Periyat, S. C. Pillai, D. E. McCormack, J. Colreavy, and S. J. Hinder, "Improved high-temperature stability and sun-light-driven photocatalytic activity of sulfur-doped anatase TiO_2," *The Journal of Physical Chemistry C*, vol. 112, no. 20, pp. 7644–7652, 2008.

[9] M. S. Wong, S. W. Hsu, K. K. Rao, and C. P. Kumar, "Influence of crystallinity and carbon content on visible light photocatalysis of carbon doped titania thin films," *Journal of Molecular Catalysis A: Chemical*, vol. 279, no. 1, pp. 20–26, 2008.

[10] J. C. Yu, J. Yu, W. Ho, Z. Jiang, and L. Zhang, "Effects of F-doping on the photocatalytic activity and microstructures of nanocrystalline TiO_2Powders," *Chemistry of Materials*, vol. 14, no. 9, pp. 3808–3816, 2002.

[11] I.-C. Kang, Q. Zhang, S. Yin, T. Sato, and F. Saito, "Novel method for preparation of high visible active N-doped TiO_2 photocatalyst with its grinding in solvent," *Applied Catalysis B: Environmental*, vol. 84, no. 3-4, pp. 570–576, 2008.

[12] X. Lin, D. Fu, L. Hao, and Z. Ding, "Synthesis and enhanced visible-light responsive of C,N,S-tridoped TiO_2 hollow spheres," *Journal of Environmental Sciences*, vol. 25, no. 10, pp. 2150–2156, 2013.

[13] M. Zhou and J. Yu, "Preparation and enhanced daylight-induced photocatalytic activity of C,N,S-tridoped titanium dioxide powders," *Journal of Hazardous Materials*, vol. 152, no. 3, pp. 1229–1236, 2008.

[14] Y. Ao, J. Xu, D. Fu, and C. Yuan, "Synthesis of C,N,S-tridoped mesoporous titania with enhanced visible light- induced photocatalytic activity," *Microporous and Mesoporous Materials*, vol. 122, no. 1-3, pp. 1–6, 2009.

[15] Y. Wang, Y. Huang, W. Ho, L. Zhang, Z. Zou, and S. Lee, "Biomolecule-controlled hydrothermal synthesis of C-N-S-tridoped TiO_2 nanocrystalline photocatalysts for NO removal under simulated solar light irradiation," *Journal of Hazardous Materials*, vol. 169, no. 1-3, pp. 77–87, 2009.

[16] Z. Li, Z. Wang, and G. Li, "Preparation of nano-titanium dioxide from ilmenite using sulfuric acid- decomposition by liquid phase method," *Powder Technology*, vol. 287, pp. 256–263, 2016.

[17] N. S. Luong, N. V. Tien, and N. V. Hung, "Research and prepare nanometer-sized titanium dioxide from Ha Tinh inmenite concentrate with sulfuric acid," *Chemistry Journal*, vol. 47, no. 2A, pp. 145–149, 2009.

[18] J. Yu, G. Dai, Q. Xiang, and M. Jaroniec, "Fabrication and enhanced visible-light photocatalytic activity of carbon self-doped TiO2sheets with exposed {001} facets," *Journal of Materials Chemistry*, vol. 21, no. 4, pp. 1049–1057, 2011.

[19] H. R. Pouretedal and M. Kiyani, "Photodegradation of 2-nitrophenol catalyzed by CoO, CoS and CoO/CoS nanoparticles," *Journal of the Iranian Chemical Society*, vol. 11, no. 1, pp. 271–277, 2014.

[20] X. Cheng, X. Yu, and Z. Xing, "Synthesis and characterization of C-N-S-tridoped TiO_2 nano-crystalline photocatalyst and its photocatalytic activity for degradation of rhodamine B," *Journal of Physics and Chemistry of Solids*, vol. 74, no. 5, pp. 684–690, 2013.

[21] T. Ohsaka, F. Izumi, and Y. Fujiki, "Raman spectrum of anatase, TiO2," *Journal of Raman Spectroscopy*, vol. 7, no. 6, pp. 321–324, 1978.

[22] V. Kiran and S. Sampath, "Enhanced Raman spectroscopy of molecules adsorbed on carbon-doped TiO_2 obtained from titanium carbide: a visible-light-assisted renewable substrate," *ACS Applied Materials & Interfaces*, vol. 4, no. 8, pp. 3818–3828, 2012.

[23] X. F. Lei, X. X. Xue, H. Yang et al., "Effect of calcination temperature on the structure and visible-light photocatalytic activities of (N, S and C) co-doped TiO_2 nano-materials," *Applied Surface Science*, vol. 332, pp. 172–180, 2015.

[24] J. Lv, T. Sheng, L. Su et al., "N, S co-doped-TiO_2/fly ash beads composite material and visible light photocatalytic activity," *Applied Surface Science*, vol. 284, pp. 229–234, 2013.

[25] N. Yao, C. Wu, L. Jia et al., "Simple synthesis and characterization of mesoporous (N, S)-codoped TiO_2 with enhanced visible-light photocatalytic activity," *Ceramics International*, vol. 38, no. 2, pp. 1671–1675, 2012.

[26] F. Dong, W. Zhao, and Z. Wu, "Characterization and photocatalytic activities of C, N and S co-doped TiO_2 with 1D nanostructure prepared by the nano-confinement effect," *Nanotechnology*, vol. 19, no. 36, p. 365607, 2008.

[27] G. Zhang, Y. C. Zhang, M. Nadagouda et al., "Visible light-sensitized S, N and C co-doped polymorphic TiO_2 for photocatalytic destruction of microcystin-LR," *Applied Catalysis B: Environmental*, vol. 144, pp. 614–621, 2014.

[28] G. Yang, Z. Yan, and T. Xiao, "Low-temperature solvothermal synthesis of visible-light-responsive S-doped TiO2 nanocrystal," *Applied Surface Science*, vol. 258, no. 8, pp. 4016–4022, 2012.

[29] Q. Xiao and L. Ouyang, "Photocatalytic photodegradation of xanthate over C, N, S-tridoped TiO_2 nanotubes under visible light irradiation," *Journal of Physics and Chemistry of Solids*, vol. 72, no. 1, pp. 39–44, 2011.

[30] X. Wang and T. T. Lim, "Solvothermal synthesis of C-N codoped TiO_2 and photocatalytic evaluation for bisphenol A degradation using a visible-light irradiated LED photoreactor," *Applied Catalysis B: Environmental*, vol. 100, no. 1-2, pp. 355–364, 2010.

[31] H. Wang and Y. Hu, "The photocatalytic property of nitrogen-doped TiO_2 nanoball film," *International Journal of Photoenergy*, vol. 2013, Article ID 179427, 6 pages, 2013.

[32] E. Grabowska, M. Marchelek, T. Klimczuk, G. Trykowski, and A. Zaleska-Medynska, "Noble metal modified TiO_2 microspheres: Surface properties and photocatalytic activity under UV-vis and visible light," *Journal of Molecular Catalysis A: Chemical*, vol. 423, pp. 191–206, 2016.

[33] K. S. W. Sing, "Reporting physisorption data for gas/solid systems with special reference to the determination of surface area and porosity (recommendations 1984)," *Pure and Applied Chemistry*, vol. 57, no. 4, pp. 603–619, 1985.

[34] M. D. Donohue and G. L. Aranovich, "A new classification of isotherms for Gibbs adsorption of gases on solids," *Fluid Phase Equilibria*, vol. 158-160, pp. 557–563, 1999.

[35] P. García-Muñoz, G. Pliego, J. A. Zazo, A. Bahamonde, and J. A. Casas, "Ilmenite ($FeTiO_3$) as low cost catalyst for advanced oxidation processes," *Journal of Environmental Chemical Engineering*, vol. 4, no. 1, pp. 542–548, 2016.

[36] D. Kibanova, M. Trejo, H. Destaillats, and J. Cervini-Silva, "Photocatalytic activity of kaolinite," *Catalysis Communications*, vol. 12, no. 8, pp. 698–702, 2011.

[37] J. M. Herrmann, "Heterogeneous photocatalysis: state of the art and present applications In honor of Pr. R.L. Burwell Jr. (1912–2003), Former Head of Ipatieff Laboratories, Northwestern University, Evanston (Ill)," *Topics in Catalysis*, vol. 34, no. 1-4, pp. 49–65, 2005.

[38] S. Kim and D. S. Aga, "Potential ecological and human health impacts of antibiotics and antibiotic-resistant bacteria from wastewater treatment plants," *Journal of Toxicology and Environmental Health, Part B*, vol. 10, no. 8, pp. 559–573, 2007.

[39] M. A. Behnajady, N. Modirshahla, M. Shokri, and B. Rad, "Enhancement of photocatalytic activity of TiO_2 nanoparticles by silver doping: photodeposition versus liquid impregnation methods," *Global NEST Journal*, vol. 10, no. 1, pp. 1–7, 2008.

[40] R. Liu, H. S. Wu, R. Yeh, C. Y. Lee, and Y. Hung, "Synthesis and bactericidal ability of TiO_2 and Ag-TiO_2 prepared by coprecipitation method," *International Journal of Photoenergy*, vol. 2012, Article ID 640487, 7 pages, 2012.

[41] J. C. Yu, W. Ho, J. Yu, H. Yip, P. K. Wong, and J. Zhao, "Efficient visible-light-induced photocatalytic disinfection on sulfur-doped nanocrystalline titania," *Environmental Science & Technology*, vol. 39, no. 4, pp. 1175–1179, 2005.

[42] A. M. Kamel, H. G. Fouda, P. R. Brown, and B. Munson, "Mass spectral characterization of tetracyclines by electrospray ionization, H/D exchange, and multiple stage mass spectrometry," *Journal of the American Society for Mass Spectrometry*, vol. 13, no. 5, pp. 543–557, 2002.

[43] J. Wang, D. Zhi, H. Zhou, X. He, and D. Zhang, "Evaluating tetracycline degradation pathway and intermediate toxicity during the electrochemical oxidation over a Ti/Ti4O7 anode," *Water Research*, vol. 137, pp. 324–334, 2018.

[44] I. Dalmázio, M. O. Almeida, R. Augusti, and T. M. A. Alves, "Monitoring the degradation of tetracycline by ozone in aqueous medium via atmospheric pressure ionization mass spectrometry," *Journal of the American Society for Mass Spectrometry*, vol. 18, no. 4, pp. 679–687, 2007.

[45] Z. Xie, Y. Feng, F. Wang et al., "Construction of carbon dots modified MoO_3/g-C_3N_4 Z-scheme photocatalyst with enhanced visible-light photocatalytic activity for the degradation of tetracycline," *Applied Catalysis B: Environmental*, vol. 229, pp. 96–104, 2018.

[46] D. Debayle, G. Dessalces, and M. F. Grenier-Loustalot, "Multi-residue analysis of traces of pesticides and antibiotics in honey by HPLC-MS-MS," *Analytical and Bioanalytical Chemistry*, vol. 391, no. 3, pp. 1011–1020, 2008.

[47] Y. Wang, H. Zhang, J. Zhang et al., "Degradation of tetracycline in aqueous media by ozonation in an internal loop- lift reactor," *Journal of Hazardous Materials*, vol. 192, no. 1, pp. 35–43, 2011.

[48] D. He, Y. Sun, L. Xin, and J. Feng, "Aqueous tetracycline degradation by non-thermal plasma combined with nano-TiO2," *Chemical Engineering Journal*, vol. 258, pp. 18–25, 2014.

[49] E. O. Oseghe and A. E. Ofomaja, "Study on light emission diode/carbon modified TiO_2 system for tetracycline hydrochloride degradation," *Journal of Photochemistry and Photobiology A: Chemistry*, vol. 360, pp. 242–248, 2018.

[50] X. Tang, Z. Wang, and Y. Wang, "Visible active N-doped TiO_2/reduced graphene oxide for the degradation of tetracycline hydrochloride," *Chemical Physics Letters*, vol. 691, pp. 408–414, 2018.

[51] X. Cao, J. Tao, X. Xiao, and J. Nan, "Hydrothermal-assisted synthesis of the multi-element-doped TiO_2 micro/nanostructures and their photocatalytic reactivity for the degradation of tetracycline hydrochloride under the visible light irradiation," *Journal of Photochemistry and Photobiology A: Chemistry*, vol. 364, pp. 202–207, 2018.

[52] X. Niu, W. Yan, C. Shao, H. Zhao, and J. Yang, "Hydrothermal synthesis of Mo-C co-doped TiO_2 and coupled with fluorine-doped tin oxide (FTO) for high-efficiency photodegradation of methylene blue and tetracycline: effect of donor-acceptor passivated co-doping," *Applied Surface Science*, vol. 466, pp. 882–892, 2019.

[53] H. R. Pouretedal and B. Afshari, "Preparation and characterization of Zr and Sn doped TiO2nanocomposite and photocatalytic activity in degradation of tetracycline," *Desalination and Water Treatment*, vol. 57, no. 23, pp. 10941–10947, 2016.

[54] X. Hu, Z. Sun, J. Song, G. Zhang, C. Li, and S. Zheng, "Synthesis of novel ternary heterogeneous BiOCl/TiO_2/sepiolite composite with enhanced visible-light-induced photocatalytic activity towards tetracycline," *Journal of Colloid and Interface Science*, vol. 533, pp. 238–250, 2019.